minerals

MDPI

Article

Petrogenesis of the Ore-Related Intrusions of the Aikengdelesite Mo (–Cu) and Halongxiuma Mo Deposits: Implication for Geodynamic Evolution and Mineralization in the East Kunlun Orogen, Northwest China

Qinglin Xu [1], Yonggang Sun [2,*], Guangzhou Mao [1], Wei Xin [1] and Yanqian Yang [3,4]

1 College of Earth Science and Engineering, Shandong University of Science and Technology, Qingdao 266590, China
2 School of Resources and Civil Engineering, Suzhou University, Suzhou 234000, China
3 Qinghai Geological Survey, Xining 810001, China
4 Technology Innovation Center for Exploration and Exploitation of Strategic Mineral Resources in Plateau Desert Region, Ministry of Natural Resources, Xining 810001, China
* Correspondence: sunyg18@mails.jlu.edu.cn

Abstract: The East Kunlun Orogenic Belt (EKOB) is the most important Triassic polymetallic metallogenic belt in China. A study about the petrogenesis of the ore-related intrusions is of great significance to the geodynamic evolution of orogenic belts. In this study, analysis of U–Pb zircon dating, whole-rock major and trace element compositions, and zircon Hf isotopes for the granitoids hosting the Aikengdelesite Mo (–Cu) and Halongxiuma Mo deposits in the EKOB are studied to determine their chronology and petrogenesis. Zircon date results show that the Aikengdelesite granite porphyry and the Halongxiuma granodiorite porphyry formed at 244.2 ± 1.7 Ma and 230.0 ± 1.0 Ma respectively. All samples of the Aikengdelesite granite porphyry and the Halongxiuma granodiorite porphyry which have high SiO_2 and K_2O contents, and low MgO and Cr, belong to the high-K calc-alkaline series. The Aikengdelesite granite porphyry samples show I-type geochemical affinities, whereas the Halongxiuma granodiorite porphyry samples are A-type granitoids. They all show negative zircon $\varepsilon_{Hf}(t)$ values (−7.4 to −3.3 and −3.7 to −2.5). We suggest that the Aikengdelesite granite porphyry may have been derived from the lower continental crust. While the Halongxiuma granodiorite porphyry could have formed by partial melting of basic lower crustal materials. By combining the results of this study with previous data, two magmatic and mineralization peak periods (278–237 Ma and 230–210 Ma) were observed in the Paleo-Tethys of the EKOB. Porphyry–skarn deposits occurring in the first episode were formed in the setting of an active continental margin related to the Paleo-Tethys Ocean plate subduction (e.g., Aikengdelesite porphyry deposit), while deposits occurring in the second episode were formed in a post-collisional setting (e.g., Halongxiuma porphyry deposit).

Keywords: geochemistry; petrogenesis; east Kunlun orogenic belt; Paleo-Tethys Ocean; geodynamic evolution

check for updates

Citation: Xu, Q.; Sun, Y.; Mao, G.; Xin, W.; Yang, Y. Petrogenesis of the Ore-Related Intrusions of the Aikengdelesite Mo (–Cu) and Halongxiuma Mo Deposits: Implication for Geodynamic Evolution and Mineralization in the East Kunlun Orogen, Northwest China. *Minerals* **2023**, *13*, 447. https://doi.org/10.3390/min13030447

Academic Editor: Rubén Díez-Fernández

Received: 16 February 2023
Revised: 7 March 2023
Accepted: 12 March 2023
Published: 22 March 2023

1. Introduction

The East Kunlun Orogenic Belt (EKOB) extends >1500 km in the east–west direction and 50–200 km in width along the northern Tibetan Plateau in northwest China (Figure 1A) [1,2]. The EKOB is characterized by a complex evolution history of the Paleo-Tethys Ocean [3,4] and records the widespread magmatism [5] rocks during the Permian–Triassic (Figure 1B) [6]. However, the tectonic setting of these magmatic rocks remains controversial. Some scholars believe that Middle Permian–Middle Triassic magmatic rocks were induced by the northward subduction of the Paleo-Tethys Ocean [7–9], whereas others have suggested that Early Triassic felsic magmatism was related to the collision between the Bayan Har–Songpanganzi Terrane and the EKOB [10–12]. Therefore, evolution of the

Paleo-Tethys from oceanic slab subduction to continental collision in EKOB, which is also an important polymetallic belt, remains to be discussed [2]. The porphyry and skarn deposits in EKOB occur mostly in Triassic granites (Figure 1B), such as the Yazigou, Hutouya, Saishitang, Yemaquan, Wulanwuzhuer, and Jiadanggen deposits [1,13]. The Aikengdelesite Mo (–Cu) and Halongxiuma Mo deposits are important breakthroughs for porphyry Mo prospecting in the eastern section of EKOB during the past decade. Many studies have been carried out, which were only published in Chinese and mainly focused on its geological characteristics [14–16], preliminary fluid inclusion analyses [17,18], geochronology, and geochemistry about the associated intrusions [16,19,20]. In addition, a consensus that the Aikengdelesite Mo (–Cu) and Halongxiuma Mo deposits are porphyry deposits has been reached. The Aikengdelesite porphyry Mo (–Cu) deposit was formed in the Early Triassic [16], and the Halongxiuma porphyry Mo deposit was formed in the Middle Triassic [21]. The tectonic setting of Triassic porphyry–skarn deposits in the EKOB is controversial, and they may be attributed either to subduction, collisional, or post-collisional setting [2,22]. Therefore, a study on petrogenesis of the Triassic Aikengdelesite and Halongxiuma ore-related intrusions can provide theoretical guidance for metallogenic research and the evolution of the Palo-Tethys Ocean in the EKOB.

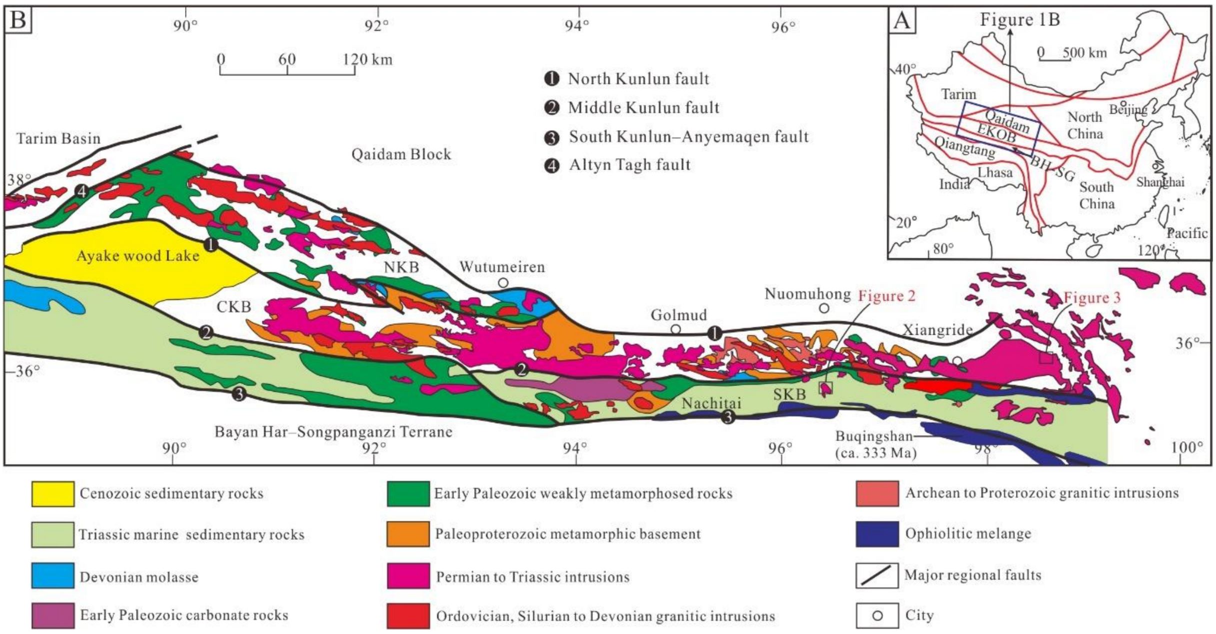

Figure 1. (**A**) Tectonic map of China (modified after [23]). EKOB, the Eastern Kunlun Orogen Belt; BH-SG, the Bayan Har–Songpanganzi Terrane; (**B**) Schematic geological map of the Eastern Kunlun Orogen Belt (modified after [1,3,7]). NKB, the North Kunlun Belt; CKB, the Central Kunlun Belt; SKB, the South Kunlun Belt.

To address the above issues, we performed zircon LA–ICP–MS U–Pb dating, whole-rock major and trace element geochemistry, and zircon Hf isotope analyses to identify the petrogenesis of granitoids hosting the Aikengdelesite Mo (–Cu) and Halongxiuma Mo deposits and associated tectonic setting. This study will also provide new constraints on the transition from Paleo-Tethys oceanic slab subduction to continental collision in the EKOB.

2. Regional Geology

The EKOB lies between the Qaidam Block in the north and the Bayan Har–Songpanganzi Terrane in the south (Figure 1A,B) [24,25]. The EKOB is divided into three parts by the North Kunlun, Middle Kunlun, and South Kunlun–Anyemaqen faults: the North Kunlun Belt (NKB), the Central Kunlun Belt (CKB), and the South Kunlun Belt (SKB) (Figure 1B) [24,25]. At least two stages of orogeny have been identified in the EKOB by previous studies:

Neoproterozoic–Early Devonian and Carboniferous–Late Triassic, corresponding to the evolution of the Proto-Tethys and Paleo-Tethys oceans, respectively [3,4,10,25,26]. Early Cambrian (522–509 Ma) and Early Carboniferous (345–333 Ma) ophiolite belts lay along the eastern section of the Middle Kunlun and South Kunlun–Anyemaqen faults record the opening of the Proto-Tethys and Palaeo-Tethys oceans, respectively (Figure 1B) [3,10,27]. The basement of the EKOB is dominated by Paleo-Mesoproterozoic middle to high grade metamorphic rocks, which consist of paragneiss, amphibolite, marble, orthogneiss, and migmatite [6,10,24,28].

The NKB is characterized by thick early Paleozoic weakly metamorphosed sedimentary clastic and carbonate rocks that are interlayered with intermediate-basic volcanic rocks [7,29,30], which are partly overlain by Devonian molasse sediments unconformably (Figure 1B). These strata are intruded by widespread Paleozoic intrusions (Figure 1B). The CKB is characterized by widespread EW-trending Permian-Triassic arc magmatic rocks, which are parallel to the Paleo-Tethys ophiolite melange belt (Figure 1B), corresponding to the evolution of the Paleo-Tethys Ocean [3,4,24,31,32]. The SKB is characterized by the early Paleozoic Naij-Tai Group, which consists of weakly metamorphosed sedimentary and volcanic rocks [10,32]. The Naij-Tai Group is overlain by Triassic marine sedimentary rocks unconformably [32]. A small number of Early Paleozoic and Mesozoic granitic bodies are exposed in SKB (Figure 1B).

It is worth mentioning that the Bayan Har–Songpanganzi Terrane is characterized by extensive coverage of huge Late Triassic turbidite sequences with thicknesses of up to 10–15 km, which were accumulated during the Ladinian through the Norian time [33,34]. This terrane thus had previously been interpreted to be floored by oceanic crust [35]. However, deep seismic investigations [36], geochemical and isotopic studies on the magmatic rocks [34], and tectonic modeling [37,38] indicate that it may currently be underlain by a South China–type continental basement at least at its eastern corner.

3. Ore Deposit Geology and Sample Descriptions

3.1. Aikengdelesite Mining Area

The Aikengdelesite porphyry Mo (–Cu) deposit is located in the eastern section of the SKB (Figure 1B). The exposed strata in the mining area comprise the Lower Triassic Hongshuichuan Formation and Quaternary sediments (Figure 2). The lithology of the Lower Triassic Hongshuichuan Formation is mainly andesite, dacite, and andesitic tuff lavas interbedded with small amounts of siliceous rocks and carbonaceous slates. Two nearly parallel EW-trending faults are distributed in the middle of the mining area (Figure 2). Multistage intrusive rocks are exposed in the Aikengdelesite mining area, including a Middle Permian medium-fine-grained monzonitic granite (ca. 268 Ma [19]), an Early Triassic medium-fine-grained syenogranite (ca. 245 Ma [16]), and a Triassic granite porphyry and medium-grained diorite (Figure 2) [14,16]. The granite porphyry intrudes the medium-fine-grained monzonitic granite rocks. The Mo–Cu orebodies in the Aikengdelesite deposit are mainly hosted within the granite porphyry. Hydrothermal alteration is extensively developed in granite porphyry and its surrounding rocks (Figure 2). The above indicates the granite porphyry, which is closely related to hydrothermal alteration of deposits, is the main host rock of the Mo–Cu mineralization. The alteration of the Aikengdelesite Mo (–Cu) deposit can be divided into potassic, silicified, phyllic, and propylitization. The first two kinds of alteration are closely associated with Mo–Cu mineralization, and the intensity of these alterations is positively related to the Mo–Cu grade. The main ore minerals of the Aikengdelesite deposit are mainly molybdenite, chalcopyrite, pyrite, and small amounts of sphalerite and galena. Gangue minerals include mainly quartz, K-feldspar, sericite, muscovite, chlorite, and calcite.

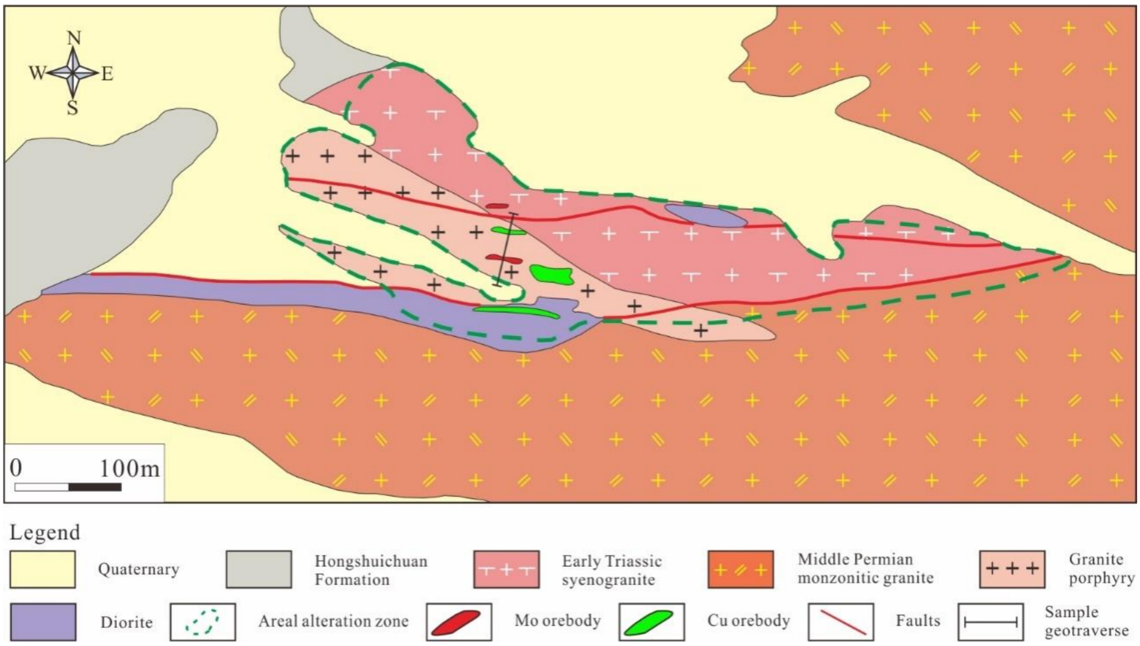

Figure 2. Geological map of the Aikengdelesite porphyry Mo (–Cu) deposit (modified from [17]).

Six fresh granite porphyry samples were collected from surface exposures (Figure 2). The granite porphyry is composed of 30–35 vol.% phenocrysts (which mainly consists of quartz (~10 vol.%), K-feldspar (~10 vol.%), plagioclase (~5 vol.%), and biotite (~5 vol.%)) and 65–70 vol.% matrix. The groundmass has the same mineral components as phenocrysts (Figure 3A,B).

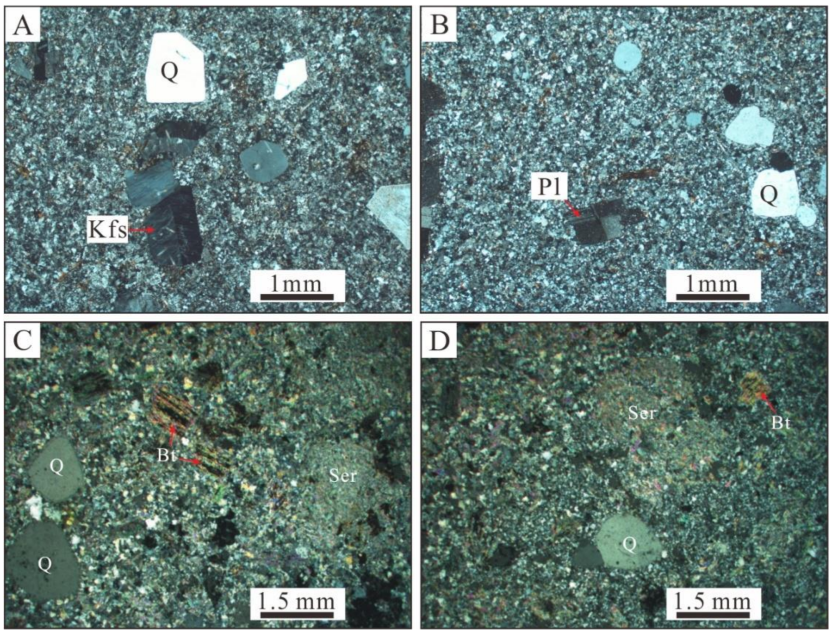

Figure 3. Photomicrographs of the ore-related porphyry bodies from the Aikengdelesite Mo (–Cu) and Halongxiuma Mo deposits. (**A**,**B**) Aikengdelesite granite porphyry with porphyritic texture; (**C**,**D**) Halongxiuma granodiorite porphyry with porphyritic texture. All photomicrographs were captured under transmitted lights. Abbreviations: Q = Quartz; Kfs = K-feldspar; Pl = Plagioclase; Bt = Biotite; Ser = Sericite.

3.2. Halongxiuma Mining Area

The Halongxiuma porphyry Mo deposit is located in the eastern section of the CKB (Figure 1B). The exposed strata in the mining area comprise the Paleoproterozoic Jinshuikou Group and Quaternary sediments (Figure 4). The lithology of the Jinshuikou Group is mainly gneiss, schist, and marble. Near-EW-trending fracture zones are developed within the Proterozoic basement (Figure 4). Multiphase magmatism occurs in the Halongxiuma mining area, mainly consisting of Early Permian granodiorite, Triassic monzonitic granite, and granodiorite porphyry (Figure 4). Porphyry Mo mineralization is developed mainly in the Triassic granodiorite porphyry bodies that intruded the Proterozoic Jinshuikou Group at or near the contact zones between the porphyry bodies and metamorphic rocks (Figure 4). Therefore, the Mo mineralization is more closely related to granodiorite porphyry bodies. In addition, Pb–Zn mineralization has also been observed in several drill cores in the Halongxiuma mining area.

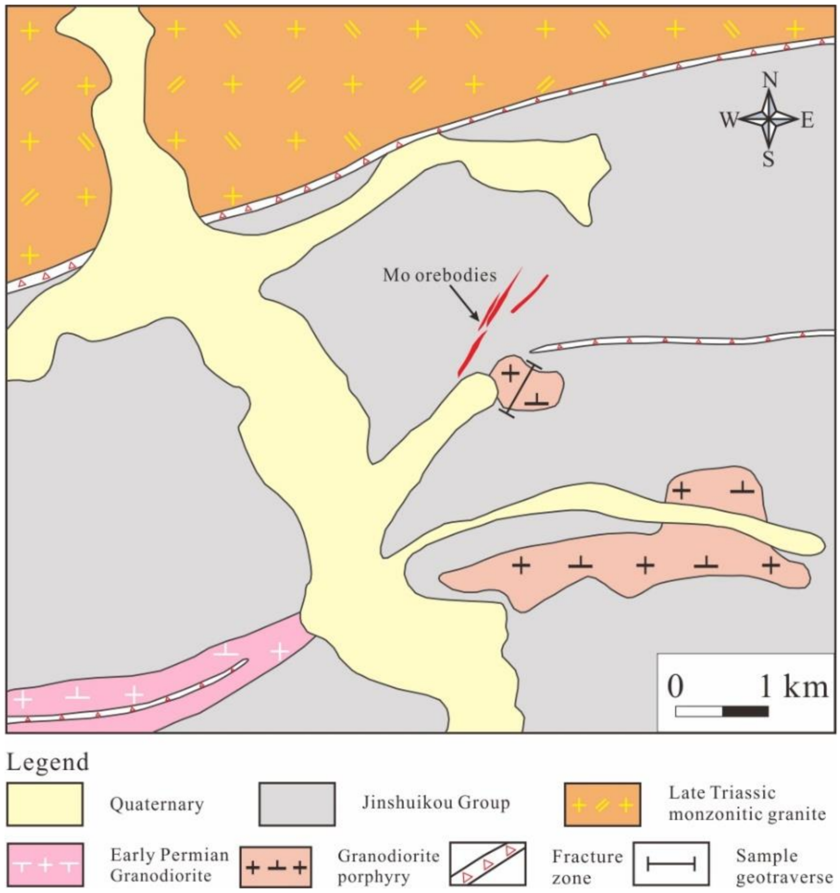

Figure 4. Geological map of the Halongxiuma porphyry Mo deposit (modified from [21]).

Five fresh granodiorite porphyry samples were collected from surface exposures (Figure 4). The granodiorite porphyry consists of ~30 vol.% phenocrysts (which are dominantly composed of quartz (~15 vol.%), plagioclase (~10 vol.%), and biotite (~5 vol.%)) and ~70 vol.% matrix. Mineral composition of the matrix is the same as that of the phenocrysts (Figure 3C,D).

4. Analytical Methods

4.1. LA–ICP–MS Zircon U–Pb Dating

The sorting of zircons was completed by the Laboratory of Langfang Regional Geology and Mineral Resources Survey. After sample crushing, magnetic separation and heavy liquid separation were adopted. Zircons with good crystal shape, with no cracks, and no obvious inclusions were selected manually through binocular microscopes. The inner structures of zircons were revealed through cathode luminescence (CL) microphotographs. Laser ablation–inductively coupled plasma–mass spectrometry (LA-ICP-MS) Zircon U-Pb dating was carried out in the Key Laboratory of institute of Mineral Resources, Chinese Academy of Geological Sciences in Beijing, using a Finnigan Neptune LA-MC-ICPMS instrument equipped with a New Wave UP 213 LA system produced by Thermo Fisher Scientific in Germany [39]. The sampling method was single point denudation with a 30 μm laser beam spot, and all signals were simultaneously received in static mode for data collection. Zircon GJ1 was used as an external standard, and zircon M127 was used as an external standard for elemental mass fraction. The method of [40] was used to correct the results for common lead. The isotope ratio and mass fraction of the samples were calculated using a 10.9 version of ICP-MS-Data Cal program [41]. Isoplot 3.0 was used to calculate the weighted-mean age and plot the concord diagram [42]. Table S1 presents the zircon U–Pb isotopic data.

4.2. Whole-Rock Major and Trace Element Analyses

The whole rock geochemical analysis was completed in the Analysis and Test Center of the Beijing Institute of Geology, Nuclear Industry. The main elements were determined by X-ray fluorescence spectrometry (XRF). The experimental instrument was the serial scanning X-ray fluorescence spectrometer PW2404 of FHLISP Company from Amsterdam, The Netherlands. The trace and rare earth elements were determined by the inductively coupled plasma mass spectrometer of ELEMENT I produced by Finnigan-MAT of Bremen, Germany. For elements greater than 20 μg/g, the error is ±5%, and for elements less than 20 μg/g, the error is ±10%. Major- and trace-element data are presented in Table S2.

4.3. Zircon Hf Isotopic Analyses

Zircon Hf isotope analysis was performed at the Key Laboratory of Mineralization and Resource Evaluation, Ministry of Land and Resources, Institute of Mineral Resources, Chinese Academy of Geological Sciences. A Finnigan Neptune Multi-receive Inductively coupled Plasma Mass Spectrometer (LA-MC-ICPMS) was used. A laser denudation system is the Newwave UP213 laser. The sampling method was single point denudation, and all signals were received simultaneously in static mode. The zircon Hf isotopes were denudated using 40–65 μm diameter spots. For details of the test process and post-processing, refer to [28,29]. The present-day chondritic ratio (CHUR) of $^{176}Hf/^{177}Hf$ = 0.282772 and $^{176}Lu/^{177}Hf$ = 0.0332 were adopted to calculate $\varepsilon_{Hf}(t)$ values [43]. In the calculation of Hf model ages, $^{176}Lu/^{177}Hf$ and $^{176}Hf/^{177}Hf$ were set as 0.0384 and 0.28325, respectively [43]. The analytical techniques and data calculated using a 10.9 version of ICP-MS Data Cal software have been described by [44]. Hf isotopic composition data are presented in Table S3.

5. Results

5.1. LA–ICP–MS Zircon U–Pb Ages

Results of zircon U–Pb dating are given in Table S1. All analyzed zircons from samples AKD-TW1 (granite porphyry) and HLXM-TW1 (granodiorite porphyry) are euhedral-subhedral (Figure 5). Their oscillatory growth zoning and the Th/U ratios (0.71–1.54) of all these analyzed zircons indicate a magmatic origin [45]. Zircons from the granite porphyry yielded $^{206}Pb/^{238}U$ ages of 251–242 Ma and a weighted-mean age of 244.2 ± 1.7 Ma (MSWD = 0.48; n = 15) (Figure 6A,B). Zircons from the granodiorite porphyry yielded $^{206}Pb/^{238}U$ ages of 231–229 Ma and a weighted-mean age of 230.0 ± 1.0 Ma (MSWD = 0.11; n = 18) (Figure 6C,D).

Figure 5. CL images of zircons from the ore-related porphyry bodies of Aikengdelesite Mo (–Cu) and Halongxiuma Mo deposits.

5.2. Whole-Rock Major and Trace Element Compositions

5.2.1. The Aikengdelesite Granite Porphyry

The whole-rock major and trace element analytical results are presented in Table S2 and illustrated in Figure 7. The six analyzed samples of the Aikengdelesite granite porphyry are characterized by relatively high SiO_2 (73.85–76.72 wt.%), Al_2O_3 (12.64–13.91 wt.%), and K_2O (4.67–5.21 wt.%), and low Na_2O (2.89–3.33 wt.%), MgO (0.13–0.28 wt.%) with $Mg^{\#}$ values of 17–29. These signatures denote the granite porphyry as high-K and calc-alkalic granite (Figure 7).

The chondrite-normalized REE patterns in all granite porphyry samples show a slightly enrichment of LREEs relative to HREEs and a moderate degree of negative Eu anomalies (Eu/Eu* = 0.42 to 0.51; Figure 8A). The granite porphyry samples exhibit enrichment in LILEs (e.g., Rb, Th, U, and K) and depletion in Ba, Nb, Sr, and Ti (Figure 8B).

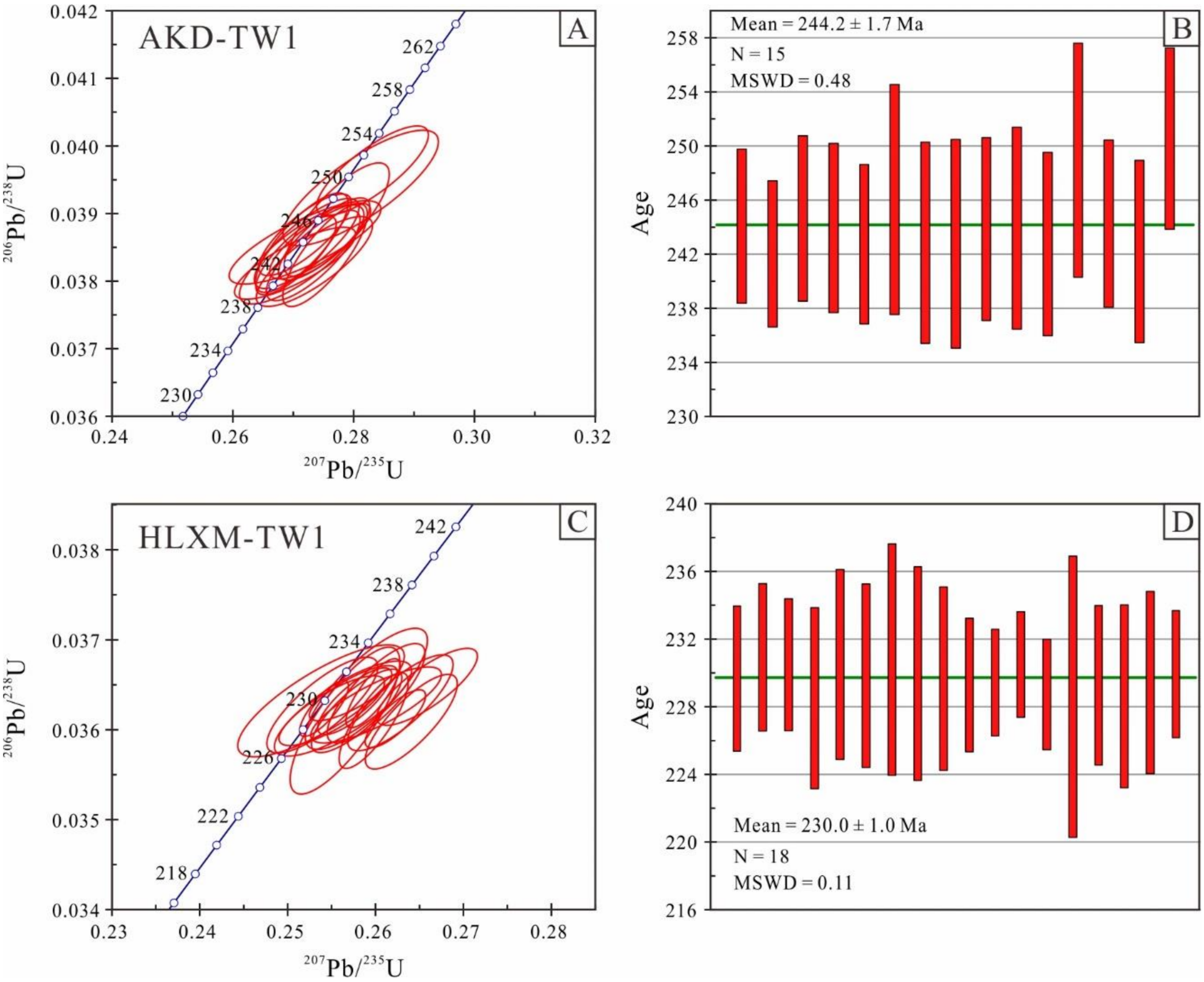

Figure 6. (**A**) Zircon U–Pb concordia diagram and (**B**) weighted mean $^{206}Pb/^{238}U$ ages for the ore-related porphyry bodies of Aikengdelesite Mo (–Cu); (**C**) Zircon U–Pb concordia diagram and (**D**) weighted mean $^{206}Pb/^{238}U$ ages for the ore-related porphyry bodies of Halongxiuma Mo deposits.

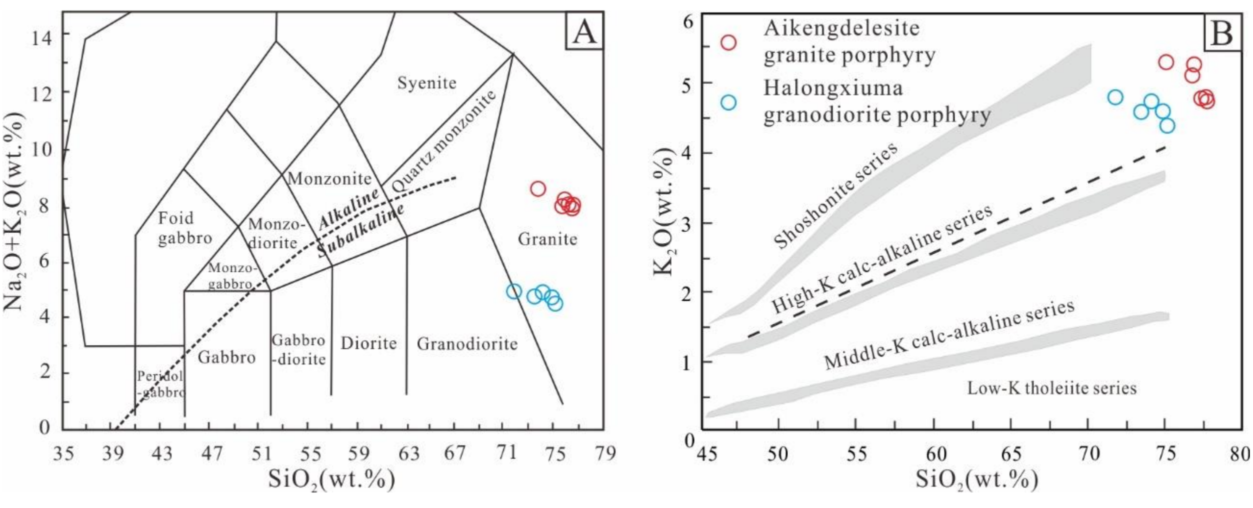

Figure 7. (**A**) TAS diagram (after [46]); (**B**) K_2O vs. SiO_2 diagram (after [47]) for the ore-related porphyry bodies from the Aikengdelesite Mo (–Cu) and Halongxiuma Mo deposits.

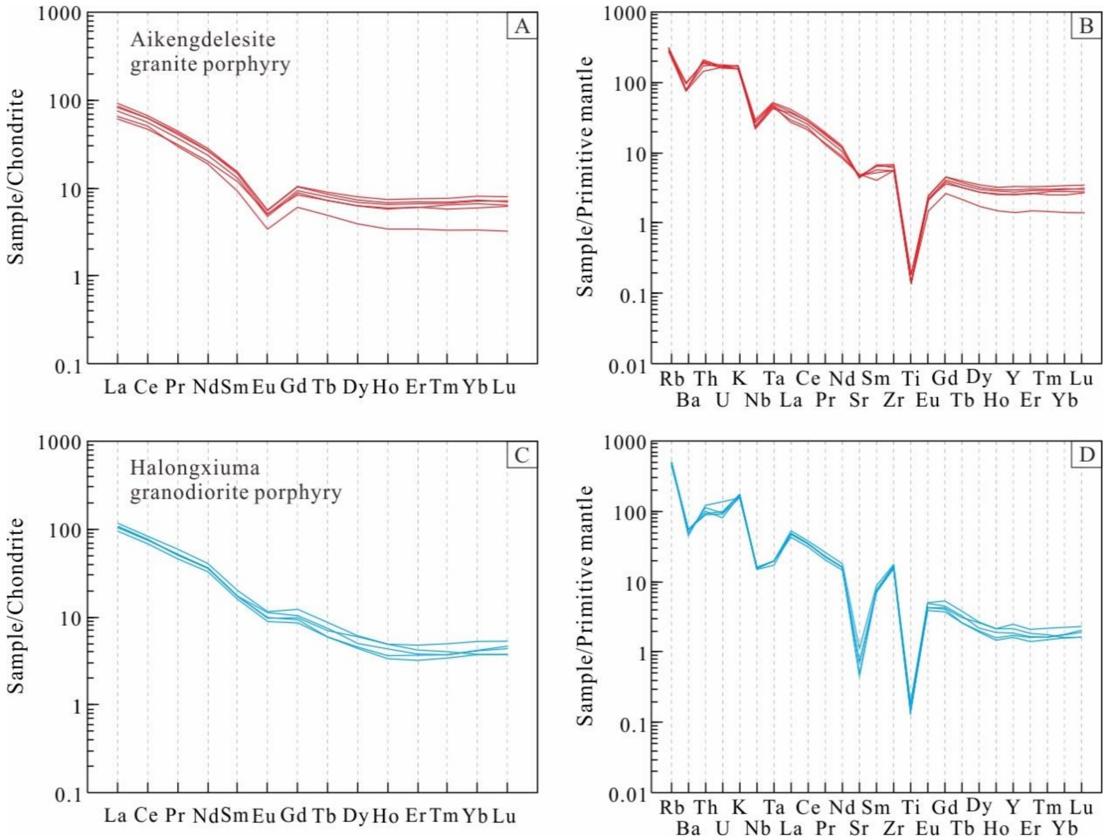

Figure 8. (**A**) Primitive mantle normalized spider diagrams and (**B**) chondrite-normalized REE patterns for the ore-related porphyry bodies from the Aikengdelesite Mo (–Cu); (**C**) Primitive mantle nor-malized spider diagrams and (**D**) chondrite-normalized REE patterns for the ore-related porphyry bodies from the Halongxiuma Mo deposits. The chondrite values are from [48], the primitive mantle values are from [49].

5.2.2. The Halongxiuma Granodiorite Porphyry

The whole-rock major and trace element analytical results are presented in Table S2 and illustrated in Figure 7. The six analyzed samples of the Halongxiuma granodiorite porphyry are characterized by relatively high SiO_2 (71.81–75.18 wt.%), Al_2O_3 (13.67–14.42 wt.%), and K_2O (4.40–4.81 wt.%), and low Na_2O (0.06–0.12 wt.%), MgO (0.64–0.85 wt.%) with $Mg^{\#}$ values of 32–48. These signatures denote the granodiorite porphyry as high-K and calc-alkalic granite (Figure 7).

The chondrite-normalized REE patterns in all granodiorite porphyry samples show a slightly enrichment of LREEs relative to HREEs and weak negative Eu anomalies (Eu/Eu* = 0.71 to 0.81; Figure 8C). The granodiorite porphyry samples exhibit enrichment in LILEs (e.g., Rb, Th, U, and K) and depletion in HFSEs (e.g., Nb, Ta, and Ti) (Figure 8D).

5.3. Zircon Hf Isotopic Compositions

In situ Lu–Hf isotope analysis was carried out for U-Pb dating of AKD-TW1 and HLXM-TW1 samples. The results are given in Table S3 and plotted in Figure 9. Ten zircon grains Lu–Hf isotope analyses for the granite porphyry (AKD-TW1) yielded $^{176}Hf/^{177}Hf$ ratios of 0.282422 to 0.282539 and negative $\varepsilon_{Hf}(t)$ values of −7.4 to −3.3. The two-stage model ages (T_{DM2}) are in the range of 1743–1483 Ma. Ten zircon grains Lu–Hf isotope analyses for the granodiorite porphyry (HLXM-TW1) yielded $^{176}Hf/^{177}Hf$ ratios of 0.282531 to 0.282563 and negative $\varepsilon_{Hf}(t)$ values of −3.7 to −2.5. The two-stage model ages (T_{DM2}) are in the range of 1494–1422 Ma.

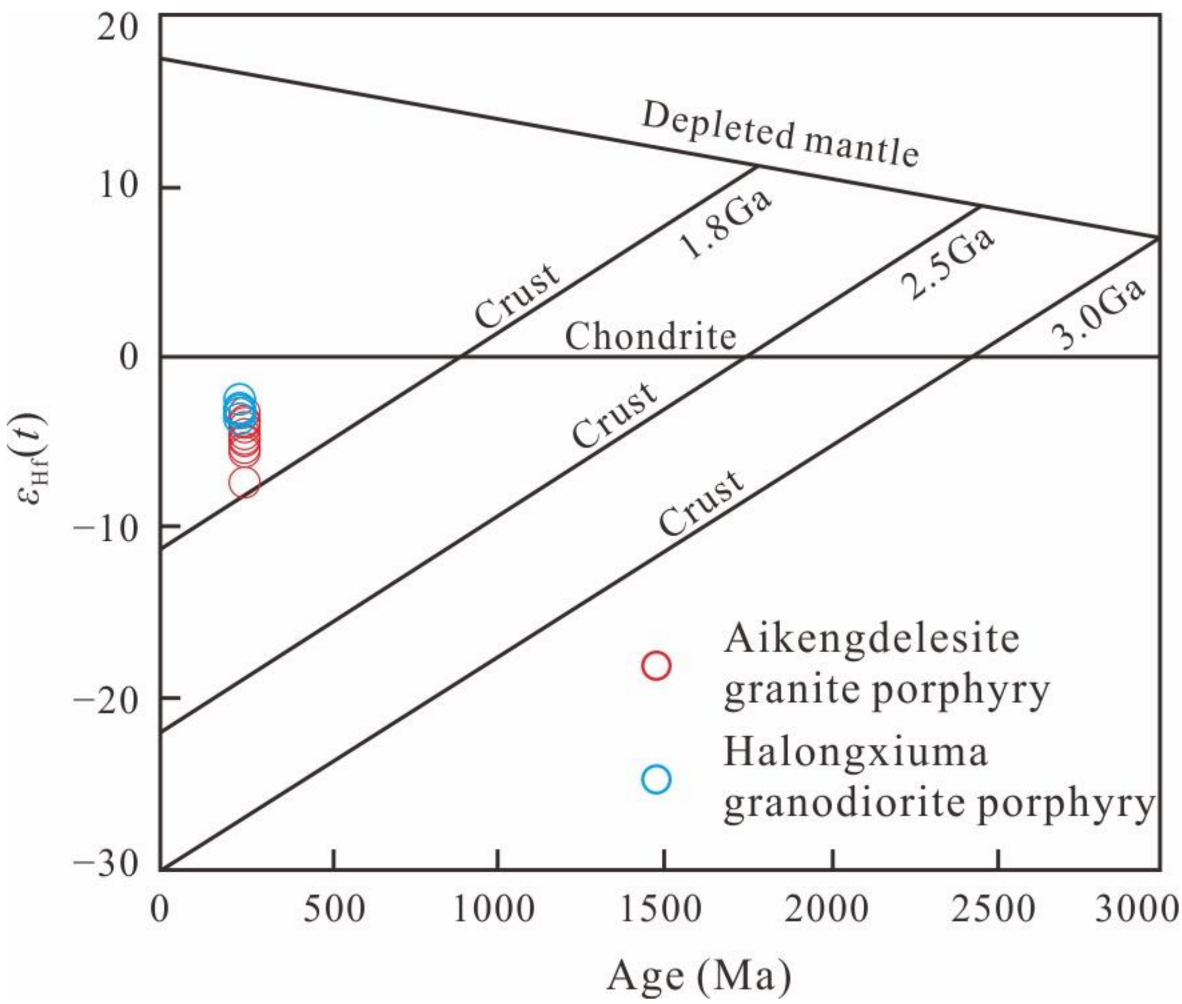

Figure 9. Plots of zircon U–Pb ages vs. $\varepsilon_{Hf}(t)$ values for the ore-related porphyry bodies from the Aikengdelesite Mo (–Cu) and Halongxiuma Mo deposits.

6. Discussion

6.1. Timing of Magmatism and Mo Mineralization

According to the geology of the Aikengdelesite Mo (–Cu) mining area, the granite porphyry is closely related to the space of ore body, indicating that the granite porphyry is genetically related to the Mo mineralization in the Aikengdelesite Mo (–Cu) deposit, providing ore-forming materials and fluid sources for mineralization. Therefore, the time of Mo mineralization (ca. 245 Ma) can be approximated as the crystallization age of the ore-related granite porphyry. Similarly, the Late Triassic granodiorite porphyry (ca. 230 Ma) is the most likely rock mass to cause porphyry Mo mineralization in the Halongxiuma Mo deposit. In addition, a large number of existing geochronological data from the EKOB [22,50–57] show that porphyry and skarn deposits constitute the Triassic Cu–Mo polymetallic metallogenic belt in this area, indicating that this area has great porphyry metallogenic potential.

6.2. Petrogenesis

For Triassic granitoids in the EKOB, enriched mantle derived melt [8,58,59], oceanic crust and overlying sediments [12], and lower crust derived melts [60] could be potential magmatic sources.

6.2.1. The Aikengdelesite Granite Porphyry

The 10,000Ga/Al ratios of the Aikengdelesite granite porphyry samples vary from 1.28 to 1.77, which are lower than the minimum value of 2.6 for typical A-type granitoids [61]. In the 10,000Ga/Al vs. Ce and 10,000Ga/Al vs. Zr diagrams (Figure 10A,B), these samples almost all plot in the overlapping region of I- and S-type granitoids. The Aikengdelesite granite porphyry samples commonly contain hydrous minerals (e.g., biotite) but carry no typical aluminum-rich minerals (e.g., muscovite, cordierite, garnet, or andalusite) (Figure 3A,B), precluding the possibility of S-type granitoids [62]. These characteristics clearly indicate that the granite porphyry samples are I-type granitoids.

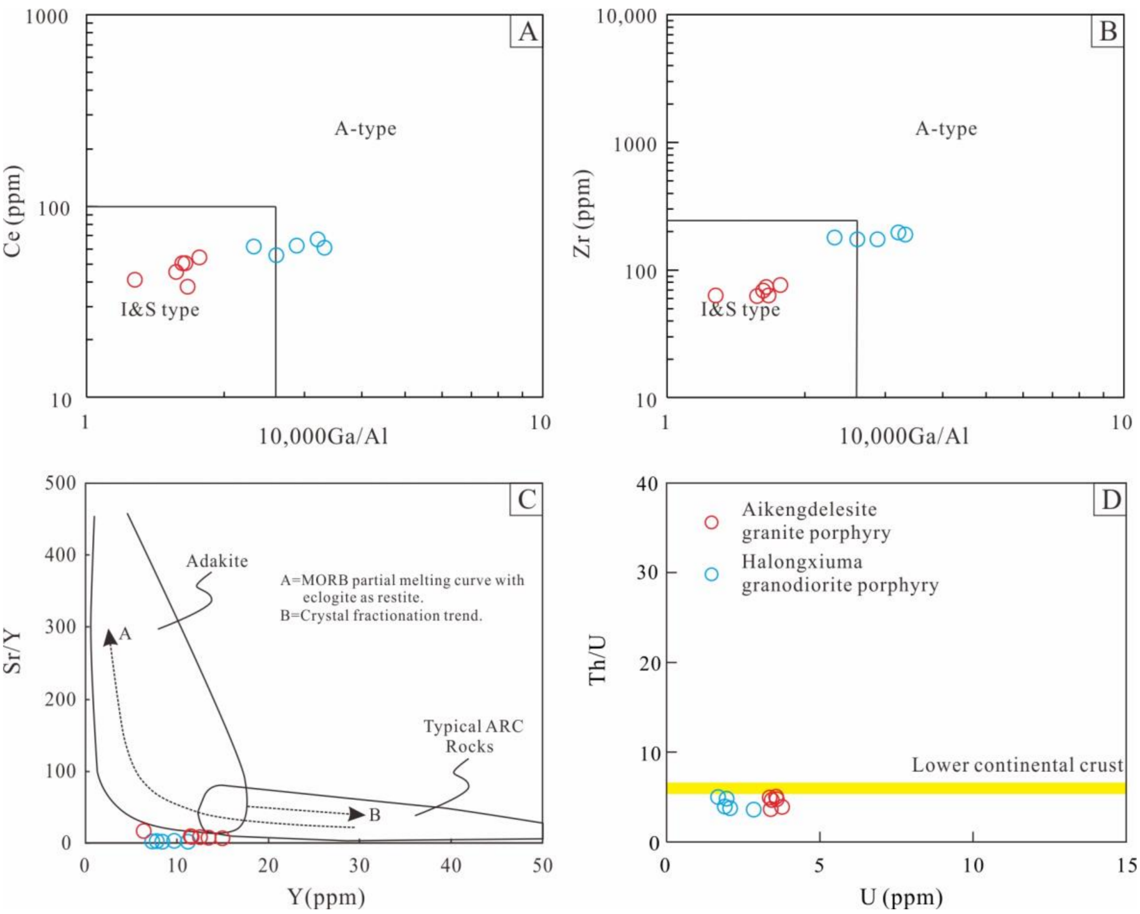

Figure 10. (**A**) 10,000Ga/Al vs. Ce; (**B**) 10,000Ga/Al vs. Zr; (**C**) Y vs. Sr/Y; and (**D**) U vs. Th/U diagrams for the ore-related porphyry bodies from the Aikengdelesite Mo (–Cu) and Halongxiuma Mo deposits. The average Th/U ratio (~6) of the lower continental crust is from [63].

The Aikengdelesite granite porphyries gave high SiO_2 (73.85–76.72 wt.%) and K_2O (4.67–5.21 wt.%), low MgO (0.13–0.28 wt.%), and Cr (3.82–6.14 ppm) contents (Table S2), implying little or no mantle contribution [64]. The Aikengdelesite granite porphyries do not have an adakitic affinity (Figure 10C). Hence, they are different in origin from adakites derived from the subducted oceanic crust. The samples of the Aikengdelesite granite porphyry belong to high-K calc-alkaline series, indicating that they are mainly crust-derived [65]. The Aikengdelesite granite porphyry samples have negative zircon $\varepsilon_{Hf}(t)$ (-7.4 to -3.3) values, which are similar to the continental crustal Hf isotope compositions (Figure 9). In addition, the Nb/Ta ratios of the Aikengdelesite granite porphyry are between 8.86 and 10.07 (average 9.34), which are lower than that of mantle derived magmas (17.5 ± 2 [66]) and close to the value of crust derived magmas (11–12 [66]), showing that the magma source area was dominated by the crust. Th/Nb ratios (0.75–1.03, average 0.87) of the Aikengdelesite granite porphyry samples reflect the crustal characteristics (average value of continental crust and primitive mantle: Th/Nb of 0.44 and 0.177, respectively [67,68]). In the U vs. Th/U plot (Figure 10D), all of the samples occur near the lower continental crust, showing that the Aikengdelesite granite porphyries were dominantly derived from the lower continental crust.

6.2.2. The Halongxiuma Granodiorite Porphyry

The Halongxiuma granodiorite porphyry samples commonly contain hydrous minerals (e.g., biotite) but carry no typical aluminum-rich minerals (e.g., muscovite, cordierite, garnet, or andalusite) (Figure 3C,D), precluding the possibility of S-type granitoids [66]. The 10,000Ga/Al ratios of the Halongxiuma granodiorite porphyry samples vary from 2.32 to 3.32, which are primarily higher than the minimum value of 2.6 for typical A-type granitoids with only one value less than 2.6 [61]. These samples also almost all plot in the region of A-type granitoids (Figure 10A,B). These characteristics clearly indicate that the granite porphyry samples are A-type granitoids.

The Halongxiuma granodiorite porphyries are characterized by display high SiO_2 (71.81–75.18 wt.%) and low MgO (0.64–0.85 wt.%) contents (Table S2), which is probably the product of partial melting of the lower crust without the interaction with the mantle. Furthermore, the granodiorite porphyries do not have the characteristics of adakites (Figure 10C). Therefore, subducted oceanic crust cannot be the main source area of the Halongxiuma granodiorite porphyries. The Halongxiuma granodiorite porphyry samples have negative zircon $\varepsilon_{\mathrm{Hf}}(t)$ (−3.7 to −2.5) values, which are similar to the continental crustal Hf isotope compositions (Figure 9). The Nb/Ta ratios of the Halongxiuma granodiorite porphyry are between 13.50 and 15.14 (average 14.18), which are lower than that of mantle derived magma (17.5 $\pm$ 2 [59]) and close to the value of crust derived magma (11–12 [66]), showing that the magma source area is dominated by the crust source. La/Nb ratios (2.70–3.19, average 2.96) and Th/Nb ratios (0.67–0.95, average 0.79) of the Halongxiuma granodiorite porphyry samples all reflect the crustal characteristics (average value of continental crust and primitive mantle: La/Nb of 2.2 and 0.94, Th/Nb of 0.44 and 0.177, respectively [67,68]). All of the Halongxiuma granodiorite porphyry samples occur near the lower continental crust (Figure 10D). Therefore, the Halongxiuma granodiorite porphyries likely formed by partial melting of basic lower crustal materials.

6.3. Implication for Geodynamic Evolution and Two Episodes of Metallogenic Events

The Kunnan-A'nyemaqen ophiolite belt is composed of the EKOB's Paleo-Tethys ophiolite, which is distributed along the south Kunlun fault [69]. The study of Buqingshan ophiolite (333 Ma [27]) in the greenstone belt shows that the Paleo-Tethys Ocean began to expand in the Early Carboniferous. Liu et al. [70] studied the age of pyroxene in Xiaomiao mafic rocks (277.8 $\pm$ 2.7 Ma), indicating the initial subduction of the Paleo-Tethys Ocean. However, the closure time of the Paleo-Tethys Ocean has been controversial. It may be Late Permian [12], Early–Middle Triassic [71], or Late Triassic [1,22,25,72].

We summarize the chronological records of Permian to Triassic igneous activities in the EKOB in recent years, finding that the magmatic activities in the EKOB have the characteristics of double peaks in age (Figure 11). The first peak is concentrated between 278 and 237 Ma, the second peak is between 230 and 210 Ma, and it is in a state of gradual attenuation between 237 and 230 Ma. There is no doubt that this phenomenon must be closely related to the geodynamic process. A large number of the Permian–Middle Triassic subduction-related magmatic rocks (278–237 Ma; Figure 11), including the granitoids with mafic microgranular enclaves (MMEs) and mafic rocks [8,12,73–76], were identified in the EKOB. All the evidence indicates that the EKOB was still in an active continental margin environment before ca. 237 Ma. Although the termination time of oceanic subduction cannot be precisely constrained by subduction-related granitoids [8], the presence of significant volumes of adakites, mafic dike swarms, and A-type granites (230–210 Ma) in the EKOB [25,60,77] clearly reveals that the Paleo-Tethys Ocean should have closed before ca. 230 Ma [78–81]. Therefore, it can be concluded that the ocean basin of the EKOB was closed at about 237 Ma, a collision occurred between 237 and 230 Ma and thickened the crust, while 230–210 Ma was the post-collisional extension stage (Figure 11). The sedimentary records in the EKOB also support this conclusion, although it has also been suggested that contact and collision never occurred due to buffering of the up to 10–15 km thick Upper Triassic flysch sequences accumulated on the Songpan–Ganzi Terrane [33,35]. The Gequ Formation (260–252 Ma) consists of oceanic molasse sediments and was deposited in an oceanic environment [82]. The Naocangjiangou and Xilikete formations (247–237 Ma) show marine facies (Figure 11). The Babaoshan Formation (237–205 Ma) above the angular unconformity shows lake or river facies (Figure 11). Therefore, all the evidence indicates that the Paleo-Tethys Ocean in the EKOB may have been open before 237 Ma, and 237 Ma probably represents the beginning of the continental collision (Figure 11).

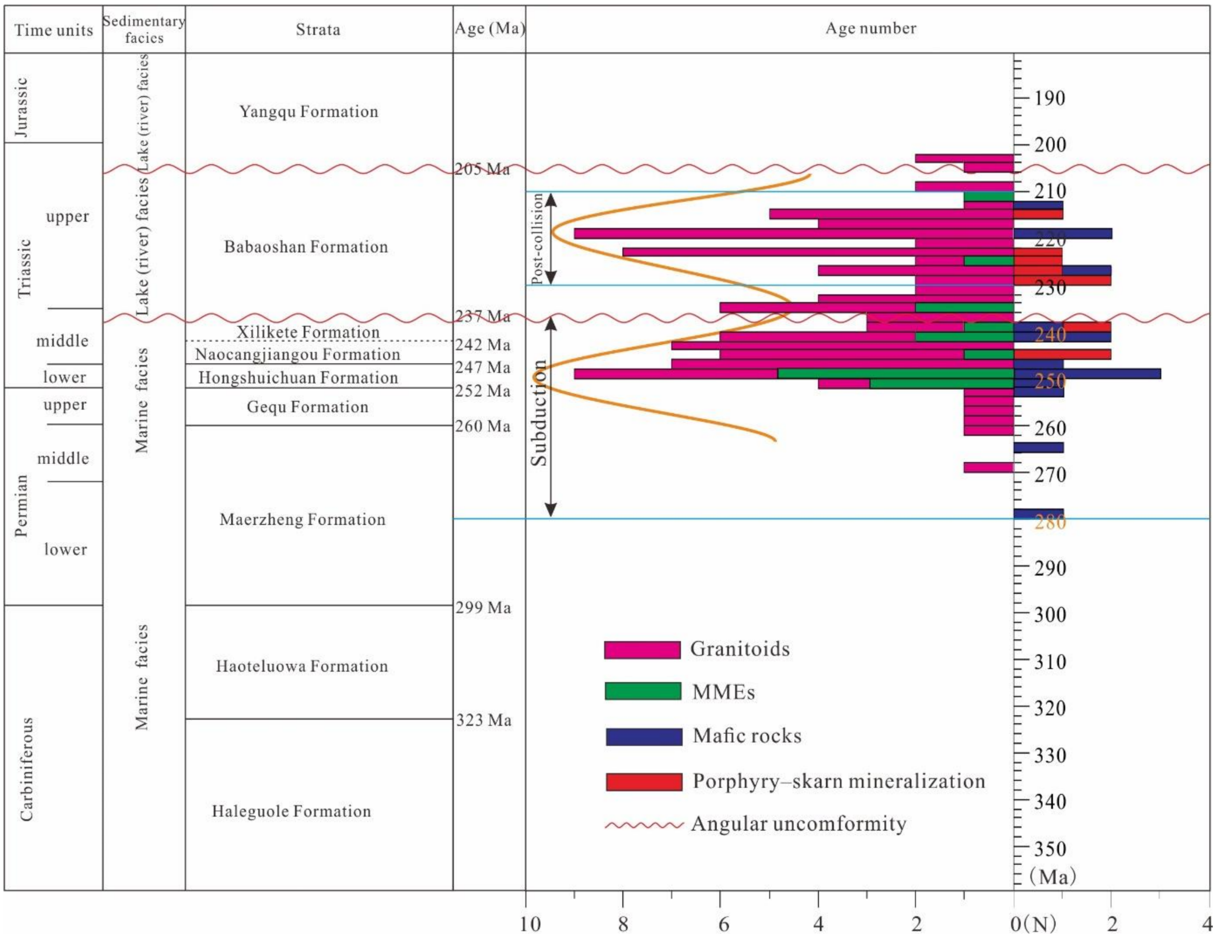

Figure 11. Histogram showing variations in the zircon U–Pb ages of the Permian–Triassic magmatic rocks in the EKOB, illustrating the geodynamic evolution of this region (modified after [60,76]).

Based on the geodynamic evolution of the Paleo-Tethys and mineralization ages for the porphyry–skarn deposits in the EKOB, two stages of metallogenic events were identified and similar to the peak age of magmatic activity (Figure 11; Table 1). The first stage of mineralization mainly occurred between 244 and 238 Ma. These porphyry–skarn deposits were formed in an active continental margin setting related to the subduction of the Paleo-Tethys Ocean plate (Figure 12A). The second episode happened after 230 Ma (230–215 Ma). These deposits were formed in a post-collisional setting (Figure 12B).

Table 1. High-precision magmatic and mineralization ages for the porphyry–skarn deposits in the EKOB.

Deposit	Type	Analytical Minerals/Rocks	Analytical Methods	Age (Ma)	Reference
Aikengdelesite	Porphyry (Cu, Mo)	Granite porphyry	Zircon LA–ICP–MS U–Pb	244.2 ± 1.7	This study
Xiadeboli	Porphyry (Cu, Mo)	Granite porphyry	Zircon SIMS U–Pb	244.2 ± 2.1	[83]
Maoniugou	Porphyry (Cu, Au)	Molybdenite	Re–Os	238.7 ± 1.4	[84]
Kaerqueka	Skarn–porphyry (Cu, Pb, Zn)	Molybdenite	Re–Os	238.8 ± 1.3	[53]
Halongxiuma	Porphyry (Mo)	Granodiorite Porphyry	Zircon LA–ICP–MS U–Pb	230.0 ± 1.0	This study
Hutouya	Skarn (Cu, Pb, Zn)	Molybdenite	Re–Os	230.1 ± 4.7	[85]
Jiadanggen	Porphyry (Cu, Mo)	Granodiorite porphyry	Zircon LA–ICP–MS U–Pb	227.0 ± 1.0	[86]
		Molybdenite	Re–Os	227.2 ± 1.9	
Yazigou	Porphyry (Cu, Mo)	Granite porphyry	Zircon SHRIMP U–Pb	224.0 ± 1.6	[87]
		Molybdenite	Re–Os	224.7 ± 3.4	
Saishitang	Skarn (Cu)	Quartz diorite	Zircon LA–ICP–MS U–Pb	222.7 ± 2.3	[88]
		Molybdenite	Re–Os	223.4 ± 1.5	
Wulanwuzhuer	Porphyry (Cu, Mo)	Granite porphyry	Zircon SHRIMP U–Pb	215.1 ± 4.5	[89]

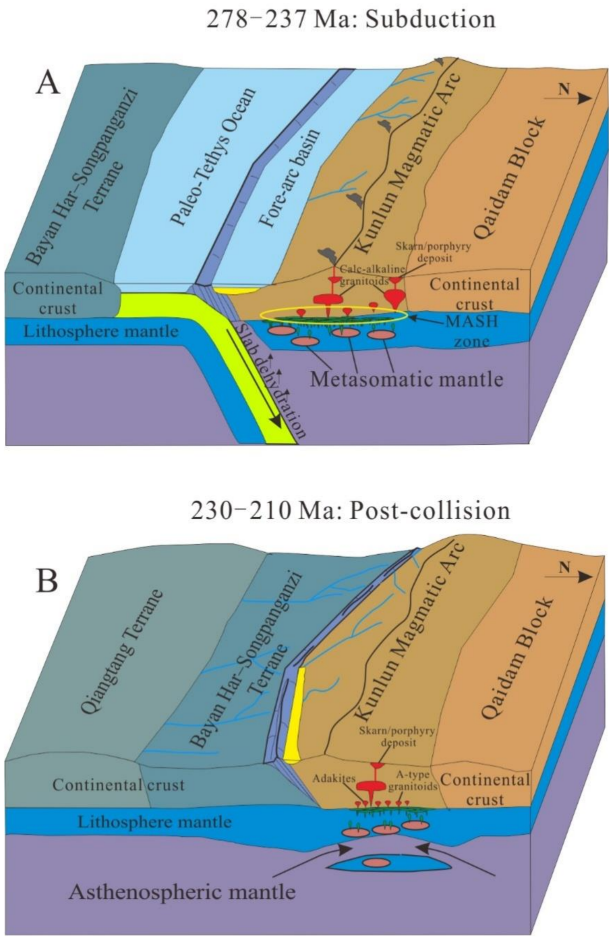

Figure 12. Schematic cartoon illustrating the Permian–Late Triassic (280–210 Ma) geodynamic evolution in the EKOB. (**A**) subduction of the Paleo-Tethys Ocean plate (278–237 Ma); and (**B**) delamination of lower lithospheric mantle (230–210 Ma).

7. Conclusions

(1) The ore-related intrusions emplaced at ca. 244 Ma for granite porphyry in the Aikengdelesite porphyry Mo (–Cu) deposit, and at ca. 230 Ma granodiorite porphyry in the Halongxiuma porphyry Mo deposit;
(2) The Aikengdelesite I-type granite porphyry samples may have been derived from the lower continental crust. The Halongxiuma granodiorite porphyry samples should be formed by partial melting of basic lower crustal materials;
(3) There are two magmatic and mineralization peak periods (278–237 Ma and 230–210 Ma), corresponding to two geodynamic evolution stages of subduction and post-collision extension, respectively.

Supplementary Materials: The following supporting information can be downloaded at: https://www.mdpi.com/article/10.3390/min13030447/s1, Table S1: LA–ICP–MS zircon U-Pb dating data for the ore-related intrusions of the Aikengdelesite Mo (–Cu) and Halongxiuma Mo deposits; Table S2: Major (wt.%) and trace element (ppm) contents for the ore-related intrusions of the Aikengdelesite Mo (–Cu) and Halongxiuma Mo deposits; Table S3: Zircon Hf isotopic date for the ore-related intrusions of the Aikengdelesite Mo (–Cu) and Halongxiuma Mo deposits.

Author Contributions: Conceptualization, Q.X., Y.S. and W.X.; software, Q.X., Y.S. and W.X.; investigation, Q.X., Y.S., W.X. and Y.Y.; data curation, Q.X., Y.S. and W.X.; funding acquisition, Q.X., Y.S. and G.M.; project administration, Q.X., Y.S. and G.M.; writing—original draft preparation, Q.X., Y.S. and W.X.; and writing—review and editing, Q.X., Y.S. and W.X. All authors have read and agreed to the published version of the manuscript.

Funding: This research was funded by the National Natural Science Foundation of China (U22A20571, 42172087, 41572063), the Shandong Provincial Natural Science Foundation of China (ZR2019PD017), the Doctoral Scientific Research Start-Up Fund Project of Suzhou University (2022BSK009), the Shandong Provincial Natural Science Foundation of China (ZR2021QD086), and the Basic Scientific Research Project of colleges and universities of Liaoning Provincial Department of education in 2021 (LJKZ0369).

Data Availability Statement: Not applicable.

Conflicts of Interest: The authors declare no conflict of interest.

References

1. Dong, Y.; He, D.; Sun, S.; Liu, X.M.; Zhou, X.H.; Zhang, F.F.; Yang, Z.; Cheng, Z.; Zhao, G.C.; Li, J.H. Subduction and accretionary tectonics of the East Kunlun Orogen, western segment of the Central China Orogenic System. *Earth Sci. Rev.* **2018**, *186*, 231–261. [CrossRef]
2. Wang, H.; Feng, C.; Li, R.; Li, D. Geological characteristics, metallogenesis, and tectonic setting of porphyry–skarn Cu deposits in East Kunlun Orogen. *Geol. J.* **2018**, *53*, 58–76. [CrossRef]
3. Yang, J.-S.; Robinson, P.T.; Jiang, C.-F.; Xu, Z.-Q. Ophiolites of the Kunlun mountains, China and their tectonic implications. *Tectonophysics* **1996**, *258*, 215–231. [CrossRef]
4. Yin, A.; Harrison, T.M. Geologic evolution of the Himalayan-Tibetan orogen. *Annu. Rev. Earth Planet. Sci.* **2000**, *28*, 211–280. [CrossRef]
5. Zeng, L.; Zhang, K.J.; Tang, X.C.; Zhang, Y.X.; Li, Z.W. Mid-Permian rifting in central China: Record of geochronology, geochemistry and Sr–Nd–Hf isotopes of bimodal magmatism on NE Qinghai–Tibetan Plateau. *Gondwana Res.* **2018**, *57*, 77–89. [CrossRef]
6. Mo, X.X.; Luo, Z.H.; Deng, J.F.; Yu, X.H. Granitoids and crustal growth in the east Kunlun orogenic belt. *Geol. J. China Univ.* **2007**, *3*, 403–414, (In Chinese with English abstract).
7. Ding, Q.F.; Liu, F.; Yan, W.; Li, B.L.; Sun, F.Y. Zircon U-Pb geochronology and Hf isotopic constraints on the petrogenesis of Early Triassic granites in the Wulonggou area of the Eastern Kunlun Orogen, Northwest China. *Int. Geol. Rev.* **2015**, *57*, 1735–1754. [CrossRef]
8. Chen, J.; Wei, J.; Fu, L.; Li, H.; Zhou, H.; Zhao, X.; Zhan, X.; Tan, J. Multiple sources of the Early Mesozoic Gouli batholith, Eastern Kunlun Orogenic Belt, northern Tibetan Plateau: Linking continental crustal growth with oceanic subduction. *Lithos* **2017**, *292–293*, 161–178. [CrossRef]
9. Zhao, X.; Fu, L.B.; Wei, J.H.; Bagas, L.; Santosh, M.; Liu, Y.; Zhang, D.H.; Zhou, H.Z. Late Permian back-arc extension of the eastern Paleo-Tethys Ocean. Evidence from the East Kunlun Orogen, Northern Tibetan Plateau. *Lithos* **2019**, *340–341*, 34–48. [CrossRef]

10. Jiang, C.F.; Yang, J.S.; Feng, B.G. (Eds.) Opening–closing evolution of the Kunlun mountains. In *Opening Closing Tectonics of Kunlun Mountain*; Geological Publishing House: Beijing, China, 1992; pp. 205–271. (In Chinese)
11. Zhang, K.X.; Zhu, Y.H.; Yin, H.F. Application of tectonic facies in geological mapping in east Kunlun orogenic belt. *Earth Sci. J. China Univ. Geosci.* **2004**, *29*, 661–666, (In Chinese with English abstract).
12. Huang, H.; Niu, Y.L.; Nowell, G.; Zhao, Z.D.; Yu, X.H.; Zhu, D.C.; Mo, X.X.; Ding, S. Geochemical constraints on the petrogenesis of granitoids in the East Kunlun Orogenic Belt, Northern Tibetan Plateau: Implications for continental crust growth through syn–collisional felsic magmatism. *Chem. Geol.* **2014**, *370*, 1–18. [CrossRef]
13. Xia, R.; Wang, C.; Min, Q.; Deng, J.; Carranza, E.; Li, W.; Guo, X.; Ge, L.; Yu, W. Molybdenite Re–Os, zircon U-Pb dating and Hf isotopic analysis of the Shuangqing Fe–Pb–Zn–Cu skarn deposit, East Kunlun Mountains, Qinghai Province, China. *Ore Geol. Rev.* **2015**, *66*, 114–131. [CrossRef]
14. Yang, Y.Q. Study on geological characteristics and genesis of Aikengdelesite molybdenum (copper) deposit, Eastern Kunlun, Qinghai Province. Master's Thesis, Jilin University, Changchun, China, 2013; pp. 1–130. (In Chinese with English abstract)
15. Wang, W. Geological and Geochemical Characteristics and Metallogenic Prognosis in Aikengdelesite District, Eastern Kunlun Mountains. Master's Degree Thesis, China University of Geosciences, Beijing, 2014; pp. 1–63. (In Chinese with English abstract)
16. Xu, Q.L. Study on Metallogenesis of Porphyry Deposits in Eastern Kunlun Orogenic Belt, Qinghai Province. Ph.D. Thesis, Jilin University, Changchun, China, 2014; pp. 1–195. (In Chinese with English abstract)
17. Yang, Y.Q.; Li, B.L.; Ma, Y.H.; Zhu, M.X. Fluid inclusion study on the Aikengdelesite Mo (Cu) ore deposit, Eastern Kunlun. *Northwestern Geol.* **2014**, *47*, 109–118. (In Chinese with English abstract)
18. Xu, Q.; Sun, F.; Li, B.; Yang, Y. Characteristics of Ore-forming Fluids and Metallogenic Model of the Halongxiuma Molybdenum Polymetallic Deposit in East Kunlun, Qinghai Province. *J. Jilin Univ. (Earth Sci. Ed.)* **2022**, *52*, 1512–1524. (In Chinese with English abstract)
19. Yang, Y.Q.; Li, B.L.; Xu, Q.L.; Zhang, B.S. Zircon U–Pb ages and its geological significance of the monzonitic granite in the Aikendelesite, Eastern Kunlun. *Northwestern Geol.* **2013**, *46*, 56–62. (In Chinese with English abstract)
20. Yang, Y.Q.; Li, B.L.; Ma, Y.J.; Tan, Y.; Bao, S.B.; Li, J.T.; Yu, X.L.; Wang, J.Y. Geochemistry and genesis of monzonitic granite from Aikengdelesite area in East Kunlun, Qinghai. *Northwestern Geol.* **2018**, *51*, 104–114. (In Chinese with English abstract)
21. Lu, H.F.; Yang, Y.Q.; He, J.; Li, J.Q. Zircon u-pb age dating for granodiorite porphyry and molybdenite Re-Os isotope dating of Halongxiuma molybdenum (tungsten) deposit in the East kunlun area and its geological significance. *J. Mineral. Petrol.* **2017**, *37*, 33–39. (In Chinese with English abstract)
22. Guo, X.; Zhou, T.; Jia, Q.; Li, J.; Kong, H. Highly differentiated felsic granites linked to Mo mineralization in the East Kunlun Orogenic Belt, NW China: Constrains from geochemistry, and Sr-Nd-Hf isotopes of the Duolongqiarou porphyry Mo deposit. *Ore Geol. Rev.* **2022**, *145*, 104891. [CrossRef]
23. Yuan, C.; Zhou, M.F.; Sun, M.; Zhao, Y.; Wilde, S.; Long, X.; Yan, D.P. Triassic granitoids in the eastern SongpanGanzi Fold Belt, SW China, magmatic response to geodynamics of the deep lithosphere. *Earth Planet. Sci. Lett.* **2010**, *290*, 481–491. [CrossRef]
24. Sun, F.Y.; Li, B.L.; Ding, Q.F.; Zhao, J.W.; Pan, T.; Yu, X.F.; Wang, L.; Chen, G.J.; Ding, Z.J. *Research on the Key Problems of Ore Prospecting in the Eastern Kunlun Metallogenic Belt*; Geological Survey Institute of Jilin University: Changchun, China, 2009. (In Chinese)
25. Ding, Q.F.; Jiang, S.Y.; Sun, F.Y. Zircon U-Pb geochronology, geochemical and Sr-Nd-Hf isotopic compositions of the Triassic granite and diorite dikes from the Wulonggou mining area in the Eastern Kunlun Orogen, NW China: Petrogenesis and tectonic implications. *Lithos* **2014**, *205*, 266–283. [CrossRef]
26. Roger, F.; Arnaud, N.; Gilder, S.; Tapponnier, P.; Jolivet, M.; Brunel, M.; Malavieille, J.; Xu, Z.; Yang, J. Geochronological and geochemical constraints on Mesozoic suturing in east central Tibet. *Tectonics* **2003**, *22*, 1037. [CrossRef]
27. Liu, Z.Q.; Pei, X.Z.; Li, R.B.; Li, Z.C.; Zhang, X.F.; Liu, Z.G.; Chen, G.C.; Chen, Y.X.; Ding, S.P.; Guo, J.F. LA–ICP–MS Zircon U–Pb geochronology of the two suites of ophiolites at the buqingshan area of the A'nyemaqen orogenic belt in the southern margin of East Kunlun and its tectonic implication. *Acta Geol.* **2011**, *85*, 185–194. (In Chinese with English abstract)
28. He, D.F.; Dong, Y.P.; Liu, X.M.; Yang, Z.; Sun, S.S.; Cheng, B.; Li, W. Tectono-thermal events in East Kunlun, Northern Tibetan Plateau: Evidence from zircon U–Pb geochronology. *Gondwana Res.* **2016**, *30*, 179–190. [CrossRef]
29. Liu, Y.J.; Genser, J.; Neubauer, F.; Jin, W.; Ge, X.H.; Handler, R.; Takasu, A. $^{40}Ar/^{39}Ar$ mineral ages from basement rocks in the Eastern Kunlun Mountains, NW China, and their tectonic implications. *Tectonophysics* **2005**, *398*, 199–224. [CrossRef]
30. Gao, X.F.; Xiao, P.X.; Jia, Q.Z. Redetermination of the Tanjianshan Group: Geochronological and geochemical evidence of basalts from the margin of the Qaidam basin. *Acta Geol.* **2011**, *85*, 1452–1463, (In Chinese with English abstract).
31. Xiao, W.J.; Windley, B.F.; Chen, H.L.; Zhang, G.C.; Li, J.L. Carboniferous-Triassic subduction and accretion in the western Kunlun, China: Implications for the collisional and accretionary tectonics of the northern Tibetan Plateau. *Geology* **2002**, *30*, 295–298. [CrossRef]
32. Yuan, C.; Sun, M.; Xiao, W.J.; Wilde, S.; Li, X.H.; Liu, X.H.; Long, X.P.; Xia, X.P.; Ye, K.; Li, J.L. Garnet-bearing tonalitic porphyry from East Kunlun, Northeast Tibetan plateau: Implications for adakite and magmas from the MASH zone. *Int. J. Earth Sci.* **2009**, *98*, 1489–1510. [CrossRef]
33. Zhang, K.J.; Li, B.; Wei, Q.G. Geochemistry and Nd isotopes of the Songpan-Ganzi Triassic turbidites, central China: Diversified provenances and tectonic implications. *J. Geol.* **2012**, *120*, 68–82. [CrossRef]

34. Zhang, Y.X.; Tang, X.C.; Zhang, K.J.; Zeng, L.; Gao, C.L. U–Pb and Lu–Hf isotope systematics of detrital zircons from the Songpan–Ganzi Triassic flysch, NE Tibetan Plateau: Implications for provenance and crustal growth. *Int. Geol. Rev.* **2014**, *56*, 29–56. [CrossRef]
35. Sengor, A.M.C. The story of Tethys: How many wives did Okeanos have? *Episodes* **1984**, *8*, 3–12. [CrossRef]
36. Wang, C.Y.; Han, W.B.; Wu, J.P.; Lou, H.; Chan, W.W. Crustal structure beneath the eastern margin of the Tibetan Plateau and its tectonic implications. *J. Geophys. Res.* **2007**, *112*, B07307. [CrossRef]
37. Zhang, K.J. Is the Songpan-Ganzi terrane (central China) really underlain by oceanic crust? *J. Geol. Soc. India* **2001**, *57*, 223–230.
38. Zhang, K.J. Escape hypothesis for the North and South China collision and the tectonic evolution of the Qinling orogen, eastern Asia. *Eclogae Geol. Helv.* **2002**, *95*, 237–247.
39. Yuan, H.L.; Gao, S.; Liu, X.M.; Li, H.M.; Gunther, D.; Wu, F.Y. Accurate U-Pb age and trace element determinations of zircon by laser ablation-inductively coupled plasma-mass spectrometry. *Geostand. Geoanal. Res.* **2004**, *28*, 353–370. [CrossRef]
40. Anderson, T. Correction of common lead in U-Pb analyses that do not report ^{204}Pb. *Chem. Geol.* **2002**, *192*, 59–79. [CrossRef]
41. Liu, Y.S.; Hu, Z.C.; Gao, S.; Günther, D.; Xu, J.; Gao, C.G.; Chen, H.H. In situ analysis of major and trace elements of anhydrous minerals by LA-ICP-MS without applying an internal standard. *Chem. Geol.* **2008**, *257*, 34–43. [CrossRef]
42. Ludwig, K.R. *User's Manual for Isoplot 3.00: A Geochronological Toolkit for Microsoft Excel 4*; Berkeley Geochronology Center Special Publication: Berkeley, CA, USA, 2003; 74p.
43. Blichert-Toft, J.; Gleason, J.D.; Télouk, P.; Albarède, F. The Lu–Hf isotope geochemistry of shergottites and the evolution of the Martian mantle–crust system. *Earth Planet Sci. Lett.* **1999**, *173*, 25–39. [CrossRef]
44. Wu, F.Y.; Yang, Y.H.; Xie, L.W.; Yang, J.H.; Xu, P. Hf isotopic compositions of the standard zircons and baddeleyites used in U-Pb geochronology. *Chem. Geol.* **2006**, *234*, 105–126. [CrossRef]
45. Hoskin, P.O.W. The composition of zircon and igneous andmetamorphic petrogenesis. *Rev. Mineral. Geochem.* **2003**, *53*, 27–62. [CrossRef]
46. Middlemost. Naming materials in the magma/igneous rock system. *Earth Sci. Rev.* **1994**, *37*, 215–224. [CrossRef]
47. Peccerillo, R.; Taylor, S. Geochemistry of Eocene calc-alkaline volcanic rocks from the Kastamonu area, Northern Turkey. *Contrib. Mineral. Petrol.* **1976**, *58*, 63–81. [CrossRef]
48. Boynton, W.V. Cosmochemistry of the rare earth elements: Meteorite studies. In *Rare Earth Element Geochemistry*; Henserson, P., Ed.; Elsevier: Amsterdam, The Netherlands, 1984; pp. 63–114.
49. Sun, S.S.; McDonough, W.F. Chemical and isotopic systematics of oceanic basalts: Implications for mantle composition and processes. *Geol. Soc. Lond. Spec. Publ.* **1989**, *42*, 313–345. [CrossRef]
50. Li, R.B.; Pei, X.Z.; Pei, L.; Li, Z.C.; Chen, G.C.; Chen, Y.X.; Liu, C.J.; Wang, M. The early Triassic Andean-type Halagatu granitoids pluton in the East Kunlun Orogen, northern Tibet Plateau: Response to the northward subduction of the Paleo-Tethys Ocean. *Gondwana Res.* **2018**, *62*, 212–226. [CrossRef]
51. Wang, S.; Feng, C.Y.; Li, S.J.; Jiang, J.H.; Li, D.S.; Su, S.S. Zircon SHRIMP U-Pb dating of granodiorite in the Kaerqueka polymetallic ore deposit, Qimantage Mountain, Qinghai Province, and its geological implications. *Geol. China* **2009**, *36*, 74–84.
52. He, S.Y.; Li, D.S.; Li, L.L.; Qi, L.Y.; He, S.F. Re-Os age of molybdenite from the Yazigou copper (molybdenum) mineralized area in eastern Kunlun of Qinghai Province, and its geological significance. *Geotecton. Metallog.* **2009**, *33*, 236–242. (In Chinese with English abstract)
53. Feng, C.Y.; Li, D.S.; Qu, W.J.; Du, A.D.; Wang, S.; Su, S.S.; Jiang, J.H. Re-Os isotopic dating of Molybdenite from the Suolajier skarn-type copper-molybdenum deposit of Qimantage Mountain in Qinghai Province and its geological significance. *Rock Miner. Anal.* **2009**, *28*, 223–227.
54. Feng, C.Y.; Li, D.S.; WU, Z.S.; Li, J.H.; Zhang, Z.Y.; Zhang, A.K.; Su, S.S. Major types, time-space distribution and metallogeneses of polymetallic deposits in the Qimantage metallogenic belt, eastern Kunlun area. *Northwestern Geol.* **2010**, *43*, 10–17.
55. Wang, L.J.; Griffin, W.L.; Yu, J.H.; O'Reilly, S.Y. U–Pb and Lu–Hf isotopes in detrital zircon from Neoproterozoic sedimentary rocks in the northern Yangtze Block: Implications for Precambrian crustal evolution. *Gondwana Res.* **2013**, *23*, 1261–1272. [CrossRef]
56. Chen, H.J.; Chen, Y.J.; Zhang, J. Zircon u-pb ages and hf isotope characteristics of the orebearing intrusion from the shapinggou molybdenum deposit, jinzhai county, anhui province. *Acta Petrol.* **2013**, *29*, 131–145.
57. Guo, X.Z.; Jia, Q.Z.; Zheng, Y.Y.; Li, J.C.; Li, Y.Z.; Kong, H.L. Re–Os isotopic dating of molybdenite from Reshui molybdenum polymetallic deposit in the East Kunlun and its geological significance. *Acta Geol. Sin.* **2016**, *90*, 2818–2829.
58. Shao, F.; Niu, Y.; Liu, Y.; Chen, S.; Kong, J.; Duan, M. Petrogenesis of triassic granitoids in the east kunlun orogenic belt, northern tibetan plateau and their tectonic implications. *Lithos* **2017**, *282–283*, 33–44. [CrossRef]
59. Kong, J.J.; Niu, Y.; Hu, Y.; Zhang, Y.; Shao, F. Petrogenesis of the triassic granitoids from the east kunlun orogenic belt, nwchina: Implications for continental crust growth from syn -collisional to post-collisional setting. *Lithos* **2020**, *364–365*, 1–17.
60. Xin, W.; Sun, F.Y.; Zhang, Y.T.; Fan, X.Z.; Wang, Y.C.; Li, L. Mafic–intermediate igneous rocks in the East Kunlun Orogenic Belt, northwestern China: Petrogenesis and implications for regional geodynamic evolution during the Triassic. *Lithos* **2019**, *346*, 105159. [CrossRef]
61. Whalen, J.B.; Currie, K.L.; Chappell, B.W. A-type granites: Geochemical characteristics, discrimination and petrogenesis. *Contrib. Mineral. Petrol.* **1987**, *95*, 407–419. [CrossRef]
62. Chappell, B.W. Aluminium saturation in I- and S-type granites and the characterization of fractionated haplogranites. *Lithos* **1999**, *46*, 535–551. [CrossRef]

63. Rudnick, R.; Gao, S. Composition of the continental crust. In *Treatise on Geochemistry*; Holland, H.D., Turekian, K.K., Eds.; Elsevier Ltd.: Amsterdam, The Netherlands, 2014; Volume 4, pp. 1–51.
64. Gao, S.; Rudnick, R.L.; Yuan, H.L.; Liu, X.M.; Liu, Y.S.; Xu, W.L.; Ling, W.L.; Ayers, J.; Wang, X.C.; Wang, Q.H. Recycling lower continental crust in the North China craton. *Nature* **2004**, *432*, 892–897. [CrossRef]
65. Liégeois, J.P.; Navez, J.; Hertogen, J.; Black, R. Contrasting origin of post-collisional high-K calc-alkaline and shoshonitic versus alkaline and peralkaline granitoids. The use of sliding normalization. *Lithos* **1998**, *45*, 1–28. [CrossRef]
66. Green, T.H. Significance of Nb/Ta as an indicator of geochemical processes in the crust-mantle system. *Chem. Geol.* **1995**, *120*, 347–359. [CrossRef]
67. Saunders, A.D.; Norry, M.J.; Tarney, J. Origin of MORB and chemically-depleted mantle reservoirs: Trace element constraints. *J. Petrol.* **1988**, *1*, 415–445. [CrossRef]
68. Weaver, B.L. The origin of ocean island basalt end-member compositions: Trace element and isotopic constraints. *Earth Planet. Sci. Lett.* **1991**, *104*, 381–397. [CrossRef]
69. Yang, J.S.; Wang, X.B.; Shi, R.D.; Xu, Z.Q.; Wu, C.L. The Dur'ngoi ophiolite in East Kunlun, northern Qinghai–Tibet Plateau: A fragment of paleo–Tethyan oceanic crust. *Geol. China* **2004**, *31*, 225–239, (In Chinese with English abstract).
70. Liu, B.; Ma, C.Q.; Zhang, J.Y.; Xiong, F.H.; Huang, J.; Jiang, H.A. 40Ar–39Ar age and geochemistry of subduction–related mafic dikes in northern Tibet, China: Petrogenesis and tectonic implications. *Int. Geol. Rev.* **2014**, *56*, 57–73. [CrossRef]
71. Zhao, X.; Fu, L.B.; Wei, J.H.; Zhao, Y.J.; Tang, Y.; Yang, B.R.; Guan, B.; Wang, X.Y. Geochemical characteristics of An'nage hornblende gabbro from East Kunlun orogenic belt and its constraints on evolution of Paleo–Tethys Ocean. *Earth Sci.* **2018**, *43*, 354–370.
72. Yu, M.; Dick, J.M.; Feng, C.Y.; Li, B.; Wang, H. The tectonic evolution of the East Kunlun Orogen, northern Tibetan Plateau: A critical review with an integrated geodynamic model. *J. Asian Earth Sci.* **2020**, *191*, 104168. [CrossRef]
73. Liu, C.D.; Mo, X.X.; Luo, Z.H.; Yu, X.H.; Chen, H.W.; Li, S.W.; Zhao, X. Mixing events between the crust-and mantle-derived magmas in Eastern Kunlun: Evidence from zircon SHRIMP II chronology. *Chin. Sci. Bull.* **2004**, *49*, 828–834. [CrossRef]
74. Xiong, F.H.; Ma, C.Q.; Zhang, J.Y.; Liu, B.; Jiang, H.A.; Huang, J. Zircon LA–ICP–MS U–Pb dating of Bairiqili gabbro pluton in East Kunlun orogenic belt and its geological significance. *Geol. Bull. China* **2011**, *30*, 1196–1202. (In Chinese with English abstract)
75. Xiong, F.H.; Ma, C.Q.; Zhang, J.Y.; Liu, B.; Jiang, H.A. Reworking of old continental lithosphere: An important crustal evolution mechanism in orogenic belts, as evidenced by Triassic I-type granitoids in the East Kunlun Orogen, northern Tibetan Plateau. *J. Geol. Soc. Lond.* **2014**, *171*, 847–863. [CrossRef]
76. Gao, H.C.; Sun, F.Y. Middle to Late Triassic granitic magmatism in the East Kunlun Orogenic Belt, NW China: Petrogenesis and implications for a transition from subduction to post-collision setting of the Palaeo-Tethys Ocean. *Geol. J.* **2021**, *56*, 3378–3395. [CrossRef]
77. Xi, R.G.; Xiao, P.X.; Wu, Y.Z.; Dong, Z.C.; Guo, L.; Gao, X.F. The geological significances, composition and age of the monzonitic granite in Kendekeke iron mine. *Northwestern Geol.* **2010**, *43*, 195–202. (In Chinese with English abstract)
78. Pan, Z.C.; Sun, F.Y.; Cong, Z.C.; Tian, N.; Xin, W.; Wang, L.; Zhang, Y.J.; Wu, D.Q. Petrogenesis and Tectonic Implications of the Triassic Granitoids in the Ela Mountain Area of the East Kunlun Orogenic Belt. *Minerals* **2022**, *12*, 880. [CrossRef]
79. Li, R.B.; Pei, X.Z.; Li, Z.C.; Pei, L.; Chen, G.C.; Liu, Z.Q.; Chen, Y.X.; Liu, C.J.; Wang, M.; Zhang, M. Paleo-Tethyan Ocean Evolution and Indosinian Orogenesis in the East Kunlun Orogen, Northern Tibetan Plateau. *Minerals* **2022**, *12*, 1590. [CrossRef]
80. Shao, F.L.; Niu, Y.L.; Kong, J.J.; Liu, Y.; Wang, G.D.; Zhang, Y. Petrogenesis and tectonic implications of the Triassic rhyolites in the East Kunlun Orogenic Belt, northern Tibetan Plateau. *Geosci. Front.* **2021**, *12*, 101243. [CrossRef]
81. Xia, R.; Wang, C.M.; Qing, M.; Li, W.L.; Carranza, E.J.M.; Guo, X.D.; Ge, L.S.; Zeng, G.L. Zircon U–Pb dating, geochemistry and Sr–Nd–Pb–Hf–O isotopes for the Nan'getan granodiorites and mafic microgranular enclaves in the East Kunlun Orogen: Record of closure of the Paleo-Tethys. *Lithos* **2015**, *234*, 47–60. [CrossRef]
82. Li, R.B.; Pei, X.Z.; Li, Z.C.; Liu, Z.Q.; Chen, G.C.; Chen, Y.X. Geological characteristics of late Palaeozoic-Mesozoic unconformities and their response to some significant tectonic events in eastern part of Eastern Kunlun. *Earth Sci. Front.* **2012**, *19*, 244–254.
83. Liu, J.N.; Feng, C.Y.; Qi, F.; Li, G.C.; Ma, S.C.; Xiao, Y. SIMS zircon U-Pb dating and fluid inclusion studies of Xiadeboli Cu–Mo ore district in Dulan County, Qinghai Province, China. *Acta Petrol.* **2012**, *28*, 679–690. (In Chinese with English abstract)
84. Chen, Y.F.; Zhang, D.; Lu, Y.C.; Liu, P.; Wang, X.J.; Fu, Y.; Li, W.; Guo, X.D. Re–Os dating of molybenite from the Maoniugou Cu–Au ore deposit in the northern part of the Ngola Mountain, Qinghai Province, and its geological significance. *Acta Geosci.* **2016**, *37*, 69–78. (In Chinese with English abstract)
85. Feng, C.Y.; Wang, S.P.; Shu, X.F.; Zhang, A.K.; Xiao, Y.; Liu, J.N.; Ma, S.C.; Li, G.C.; Li, D.X. Isotopic chronology of the Hutouya skarn lead–zine polymetallic ore district in Qimantagh area of Qinghai Province and its geological significance. *J. Jilin Univ.* **2011**, *41*, 1806–1817. (In Chinese with English abstract)
86. Li, B.L.; Zhi, Y.B.; Zhang, L.; Ding, Q.F.; Xu, Q.L.; Zhang, Y.J.; Qian, Y.; Wang, G.; Peng, B.; Ao, C. U–Pb dating, geochemistry, and Sr–Nd isotopic composition of a granodiorite porphyry from the Jiadanggen Cu–(Mo) deposit in the Eastern Kunlun metallogenic belt, Qinghai Province, China. *Ore Geol. Rev.* **2015**, *67*, 1–10. [CrossRef]
87. Li, S.J.; Sun, F.Y.; Wang, L.; Li, Y.C.; Liu, Z.H.; Su, S.S.; Wang, S. Fluid inclusion studies of porphyry copper mineralization in Kaerqueka polymetallic ore district, East Kunlun Mountains, Qinghai Province. *Miner. Depos.* **2008**, *27*, 399–402. (In Chinese with English abstract)

88. Wang, H.; Feng, C.Y.; Li, D.X.; Li, C.; Ding, T.Z.; Liao, F.Z. Geology, geochronology and geochemistry of the Saishitang Cu deposit, East Kunlun Mountains, NW China: Constraints on ore genesis and tectonic setting. *Ore Geol. Rev.* **2016**, *72*, 43–59. [CrossRef]
89. She, H.Q.; Zhang, D.Q.; Jiang, X.Y.; Guan, J.; Zhu, H.P.; Feng, C.Y.; Li, D.X. Geological characteristics and genesis of the Ulan Uzhur porphyry copper deposit in Qinghai. *Geol. China* **2007**, *34*, 306–314. (In Chinese with English abstract)